Enhancement of Vehicle Ride Quality Through Semi-Active Suspension: A Full-Scale Quarter-Car Test Rig Evaluation

Mohsin N. Hamzah[*], Ammar S. Merza, Bahaa-Aldin R. Abdullah

Mechanical Engineering Department, University of Technology- Iraq, 10001 Baghdad, Iraq

[*] Correspondence: Mohsin N. Hamzah (mohsin.n.hamzah@uotechnology.edu.iq)

Abstract: In the pursuit of optimizing automotive suspension systems, a semi-active suspension system (SASS) utilizing continuous skyhook control has been developed to enhance vehicle ride comfort and handling. This system is specifically engineered to mitigate vibrations stemming from high-frequency road excitations. Central to this advancement is the introduction of an electrohydraulic (EH) damper, which is uniquely characterized by solenoid valves capable of adjusting the orifice size to modify damping characteristics. By tuning the damping ratio, the system effectively minimizes the positional oscillations of the sprung mass in response to road irregularities. The dynamic behavior of this damper is comprehensively modeled through a boundary model approach, ensuring precise simulation and prediction of performance. A full-scale quarter-car test platform was constructed to evaluate the dynamic response and the efficacy of various control strategies implemented within the SASS. The performance assessments were conducted using MATLAB Simulink to simulate the behavior of the system under skyhook control algorithms, which aim to maintain the chassis's vertical stability during disturbances. Comparative tests involving a single EH damper have demonstrated a high level of correlation with the simulated models, achieving a 95% agreement level. These findings underscore the capability of the SASS to surpass traditional hydraulic dampers in terms of performance, cost-efficiency, and versatility in testing applications. The insights garnered from this study not only validate the functionality of the proposed system but also contribute significantly to the body of knowledge in vehicle dynamics and control. This research provides a foundational framework for future exploration and potential implementation of advanced damping systems in the automotive industry.

Keywords: Skyhook control strategy; Vehicle dynamics; Test platform; Semi-active suspension system; EH damper

1 Introduction

The suspension system is vital for any vehicle as it isolates the vehicle frame from road irregularities, impacting handling performance and ride comfort. To ensure consistent tire-road contact, the damper plays a crucial role in the suspension system by absorbing shocks from road imperfections and converting the energy into heat via a viscous fluid [1, 2]. Automotive suspension systems can be classified into three main types: passive, active, and semi-active, each of which has distinct impacts on vehicle performance and design. Passive systems use fixed mechanical components and offer simplicity, but they lack adaptability and require balancing track stability with road comfort. Active systems use actuators and control systems such as pneumatic, magnetorheological (MR), electrorheological (ER), or hydraulic systems, providing enhanced dynamics but consuming significant energy. However, semi-active systems offer a middle ground by adjusting damping in real-time using sensors and control technologies, leading to improved ride quality and control with lower energy consumption. Technologies such as MR fluids, solenoid valves, and piezoelectric actuators provide variable damping, but challenges like MR fluid degradation, sealing issues, and temperature sensitivity remain. Understanding the differences between these systems is essential for optimizing vehicle performance while considering energy efficiency and design constraints.

In recent years, the SASS has garnered significant interest from academic and industrial researchers. Many studies in this area have concentrated on computing the expected force from road disturbances rather than directly targeting shock reduction for passengers. Various innovative approaches have been proposed to improve these systems. For example, Huang et al. [3] developed a non-linear model for suspension systems, while Chen et al. [4] introduced a

force-tracking method. Ren et al. [5] enhanced vehicle stability by integrating skyhook and ground-hook control logic, and Tang et al. [6] implemented a state observer-based Takagi-Sugeno fuzzy controller. Rao and Kumar [7] applied the Linear Quadratic Regulator (LQR) as a control strategy for semi-active suspensions. Ab Talib and Mat Darus [8] designed an intelligent damper by suspending magnetic polarizable particles in liquid form, and then optimized the IFL controller using the Firefly Algorithm (FA) and Particle Swarm Optimization (PSO) techniques. Their study demonstrated improvements in ride comfort and reductions in body displacement, acceleration, suspension deflection, and tire deflection compared to uncontrolled systems. Gad et al. [9] optimized a semi-active seat suspension system using a multi-objective genetic algorithm (MOGA) for fractional-order PID controller gains. This system, which includes an MR damper, provides better ride comfort than traditional PID and passive seat suspension systems. Devdutt and Aggarwal [10] explored the use of an MR shock absorber in the secondary suspension system of a quarter-car model. A forward and inverse fuzzy controller was designed, and simulation results showed that the semi-active quarter-car system improved ride comfort and safety. Turnip and Hong [11] utilized sequential quadratic programming to optimize damping coefficients for a SASS, enhancing ride comfort, road holding, and noise reduction compared to passive systems. Poussot-Vassal et al. [12] analyzed the structural properties of a single-corner model, establishing benchmarks for various semi-active control strategies. Crews et al. [13] employed a MOGA to explore controller performance limits, demonstrating effectiveness in temperature mitigation and ride quality. Feng et al. [14] introduced a neural network and PID-based control algorithm, reducing vehicle vibration and enhancing ride quality. Dong et al. [15] compared five control algorithms for MR suspension, favoring sliding mode control. Biglarbegian et al. [16] developed a neuro-fuzzy control strategy, improving ride comfort, handling, and stability. Yao and Zheng [17] proposed a model reference sliding mode controller, achieving superior ride quality and robustness against uncertainties and disturbances.

The primary objective of this study is to investigate the utilization of EH dampers to adjust the damping characteristics of suspension systems. In contrast to MR and ER fluids, EH dampers employ solenoid valves to alter orifice size, enabling the adjustment of the damping ratio. EH dampers present a viable solution for vehicle applications and offer numerous advantages over alternative technologies. However, each technology possesses distinct features and parameters, including response time, controllability range, reliability, cost, weight, and maintenance requirements. Consequently, selecting the appropriate technology necessitates a comprehensive understanding of the specific application and its corresponding requirements.

2 Methodology

2.1 Quarter-Car Mathematical Model

Figure 1 shows a quarter-car model used in this study that encompasses a sprung mass (m_s) and an unsprung mass (m_{us}), connected by a semi-active damper and a spring with a stiffness coefficient k_s. The wheel tire is represented by a spring with a stiffness coefficient k_t. The positions of the unsprung and sprung masses are denoted by z_1 and z_2, respectively, while the road profile is denoted by z_0. The control force, f_d, is utilized to actuate and regulate the system.
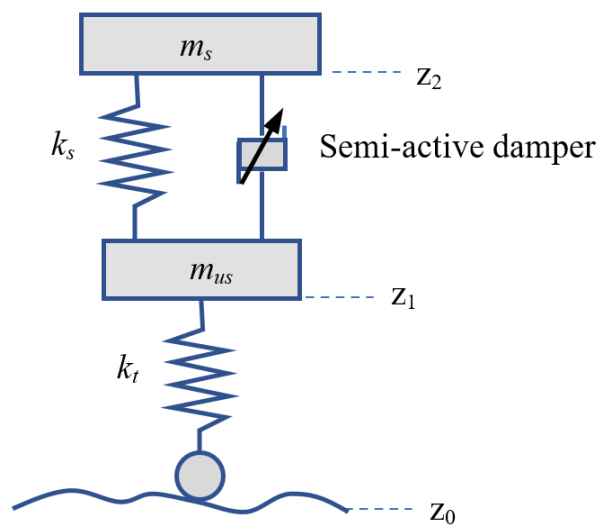

Figure 1. A semi-active suspension model

It is postulated that the wheel adheres to the road profile to sustain contact. The equations dictating the dynamics of the quarter-vehicle model are derived and expressed as follows [18]:

$$m_s \ddot{z}_2 + c (\dot{z}_2 - \dot{z}_1) + k_s (z_2 - z_1) + f_d = 0 \tag{1}$$

$$m_{us} \ddot{z}_1 - c (\dot{z}_2 - \dot{z}_1) + z_1 (k_t + k_s) - k_t z_o - k_s z_2 - f_d = 0 \tag{2}$$

2.2 State Space Model

As shown in Figure 1, the state space of the model is $x_1 = z_1, x_2 = z_2, x_3 = \dot{z}_1, x_4 = \dot{z}_2$. As a result, the state equations of the system can be expressed as follows:

$$\dot{x} = \mathbf{A}X + \mathbf{B}U \tag{3}$$

$$\dot{x} = [\dot{x}_1, \dot{x}_2, \dot{x}_3, \dot{x}_4] ; U = [z_o, f_d] \tag{4}$$

where,

$$\dot{x}_1 = 0 \times x_1 + 0 \times x_2 + x_3 + 0 \times x_4 \tag{5}$$

$$\dot{x}_2 = 0 \times x_1 + 0 \times x_2 + 0 \times x_3 + x_4 \tag{6}$$

$$\dot{x}_3 = \frac{-k_t + k_s}{m_{us}} x_1 + \frac{k_s}{m_{us}} x_2 - \frac{c}{m_{us}} x_3 + \frac{c}{m_{us}} x_4 \tag{7}$$

$$\dot{x}_4 = \frac{k_s}{m_s} x_1 - \frac{k_s}{m_s} x_2 + \frac{c}{m_s} x_3 - \frac{c}{m_s} x_4 \tag{8}$$

This expression can be represented in matrix form as follows:

$$\begin{bmatrix} \dot{x}_1 \\ \dot{x}_2 \\ \dot{x}_3 \\ \dot{x}_4 \end{bmatrix} = \begin{bmatrix} 0 & 0 & 1 & 0 \\ 0 & 0 & 0 & 1 \\ \frac{-k_t+k_s}{m_{us}} & \frac{k_s}{m_{us}} & \frac{-c}{m_{us}} & \frac{c}{m_{us}} \\ \frac{k_s}{m_s} & \frac{-k_s}{m_s} & \frac{c}{m_s} & \frac{-c}{m_s} \end{bmatrix} \begin{bmatrix} x_1 \\ x_2 \\ x_3 \\ x_4 \end{bmatrix} + \begin{bmatrix} 0 & 0 \\ 0 & 0 \\ \frac{k_t}{m_{us}} & \frac{1}{m_{us}} \\ 0 & \frac{-1}{m_s} \end{bmatrix} U \tag{9}$$

with

$$A = \begin{bmatrix} 0 & 0 & 1 & 0 \\ 0 & 0 & 0 & 1 \\ \frac{-k_t+k_s}{m_{us}} & \frac{k_s}{m_{us}} & \frac{-c}{m_{us}} & \frac{c}{m_{us}} \\ \frac{k_s}{m_s} & \frac{-k_s}{m_s} & \frac{c}{m_s} & \frac{-c}{m_s} \end{bmatrix}, \text{ and } B = \begin{bmatrix} 0 & 0 \\ 0 & 0 \\ \frac{k_t}{m_{us}} & \frac{1}{m_{us}} \\ 0 & \frac{-1}{m_s} \end{bmatrix} \tag{10}$$

where, A and B are the state matrix and the input matrix, respectively.

The system's output can be articulated as:

$$Y = \mathbf{C}X + \mathbf{D}U \tag{11}$$

where,

$$C = \begin{bmatrix} -k_s & 0 & 0 & 0 \\ \frac{k_s}{m_s} & \frac{-k_s}{m_s} & \frac{c}{m_s} & \frac{-c}{m_s} \\ 1 & -1 & 0 & 0 \end{bmatrix}, \text{ and } D = \begin{bmatrix} k_t & 0 \\ 0 & \frac{-1}{m_s} \\ 0 & 0 \end{bmatrix} \tag{12}$$

where, C denotes the output matrix, and D represents the direct transmission matrix.
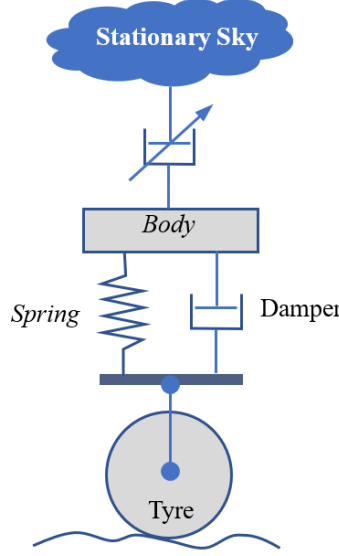
Figure 2. Definition of an ideal skyhook damper

2.3 Skyhook Control for the SASS

The current suspension system utilizes skyhook control, offering advantages over conventional models. While skyhook control typically exhibits linear characteristics, practical constraints require a tailored control strategy. Previous research has suggested approximating skyhook behavior by applying control forces between system masses [19]. To optimize ride and handling, a skyhook controller was employed in this study to adjust damping forces, enhancing suspension dynamics. Figure 2 illustrates this method, known for its simple control algorithm. Skyhook control adjusts the damping coefficient in response to changes in vehicle body velocity and other factors. This dynamic adjustment effectively minimizes the resonant peak of the sprung mass, leading to an enhanced ride experience [20].

The concept of skyhook control originated with the use of controllable semi-active dampers, which have adjustable damping capabilities ranging from firm to soft [21]. Karnopp et al. [22] first proposed the idea in 1974, conceptualizing a damper as a fixed point in the sky, hence the term "skyhook." However, given the impracticality of this notion, the control mechanism approximates an ideal skyhook [23] to achieve the desired performance.

The force exerted on the sprung mass by the skyhook damper is as follows:

$$F_{sky} = c_{\text{sky}} \, x_b \tag{13}$$

where, F_{sky} is the skyhook force.

When the sprung and unsprung masses move in opposite directions, tension occurs within the semi-active damper. The tension exerts a force on the sprung mass, altering its motion.

$$f_{sky} = (\dot{x}_b - \dot{x}_w) \tag{14}$$

where, f_{sky} is the force applied to the sprung mass. To replicate the skyhook suspension, a force in the correct direction needs to be generated.

$$C = \frac{c_{sky}\dot{x}_b}{(\dot{x}_b - \dot{x}_w)} \tag{15}$$

The damping force in a SASS typically operates in the opposite direction from the skyhook damping force. Therefore, optimizing performance requires minimizing the damping force. It's important to highlight that the damper force opposes suspension movement. In the continuous skyhook method, the low state involves a reduced damping value, while the high state is determined by maximizing the low state and the minimum ratio between the sprung mass velocity and relative velocity, multiplied by the sprung mass velocity [24].

$$C = \begin{cases} C_{\text{max}} \text{ if } \dot{X}_b \times \left(\dot{X}_b - \dot{X}_w \right) \geq 0 \\ C_{\text{min}} \text{ else } \dot{X}_b \times \left(\dot{X}_b - \dot{X}_w \right) < 0 \end{cases} \tag{16}$$

where, $x_b = z_2$ and $x_w = z_1$.

The skyhook system proposed in this study employs a two-state control scheme referred to as an ON-OFF control system. This approach toggles between high and low damping states to fulfill the necessary body comfort criteria [25]. Notably, it is essential to highlight that the semi-active damping force is correlated with the velocity of the sprung mass. Specifically, the damping force is proportional when the product of the velocities is positive, whereas it reaches a minimum when the product is negative. C_{max} is the damper's maximum damping coefficient ($C_{max} = C$), and C_{min} is the minimum one. Both values are chosen as C_{max} = 2000 N.s/m and C_{min} = 1100 N.s/m [26]. When simulating semi-active suspensions, it's crucial to carefully select the maximum and minimum damping coefficients, as they greatly impact the design of each control strategy.

2.4 Flow Dynamics of External Valves

The initial model for the external valves is based on an understanding of the fluid dynamics that occur between the chambers of the damper. This involves taking into account the principles of mass, energy, and momentum conservation in order to formulate the equation of motion for the fluid. To calculate the oil flow through the external valves once they are activated, the first step is to consider the streamline between two sections. The flow rate through the valves is then determined by applying Bernoulli's principle to a non-viscous fluid and factoring in the command voltage signals. It is assumed that the fluid has a uniform density, and that the pressure (p) and volume (V) are consistent across the cross-sections Ai. For a frictionless flow scenario, the integral form of the unsteady frictionless flow equation along a streamline between sections A_1 and A_2 can be derived as follows [23]:

$$\int_1^2 \frac{\partial v}{\partial t} ds + \int_1^2 \frac{\partial p}{\partial \rho} ds + \frac{1}{2}\left(v_2^2 - v_1^2\right) + g\left(h_2 - h_1\right) = 0 \tag{17}$$

$g\left(h_2 - h_1\right)$ represents the potential energy of the fluid and is not taken into account in the subsequent analysis. Figure 3 provides a schematic representation of the situation under discussion.
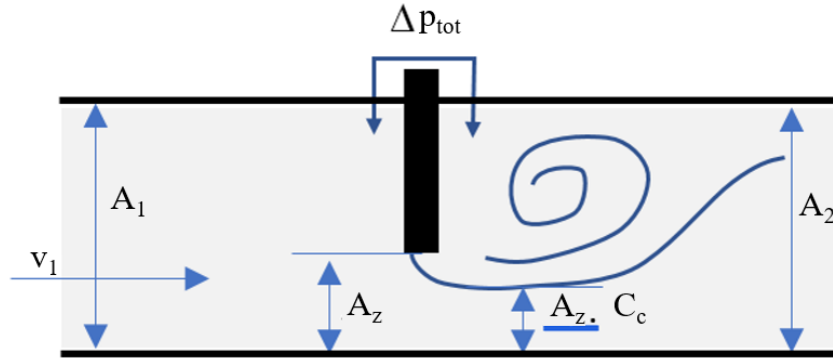

Figure 3. External valve scheme

Assuming that the flow is steady and incompressible, which means that the fluid density is constant, the integrals can be simplified to constants. By considering pressure drop (ΔH) across the valve and losses due to friction along the valve tube (JL), the equation describing steady and incompressible flow along a streamline can be reformulated as follows:

$$p_1 + \frac{1}{2}\rho v_1^2 = p_2 + \frac{1}{2}\rho v_2^2 + \Delta H + JL \tag{18}$$

where, ΔH denotes the pressure drop that occurs locally as a result of the valve, while JL represents the pressure loss that is distributed along the length of the tube.

$$\Delta H = \frac{(v_1 - v_2)^2}{2g} = \frac{v_1^2}{2g}\left(\frac{1}{m \cdot c} - 1\right)^2 \tag{19}$$

The parameter m signifies the ratio of the area of the constriction to the total area of the flow passage, with $m = A_z/A_1$. The constriction factor C accounts for the pressure drop caused by the valve, while the loss effect JL depends on the geometry of the flow passage and the Reynolds number. This description only considers the case of laminar flow for simplicity. The pressure loss due to flow resistance can be expressed as a function of the velocity in the section upstream of the valve.

$$JL = \xi \frac{64}{Re} v_1 \tag{20}$$

The variable ξ is used to denote the shape and size of the tube that connects the valves with the compression or rebound chamber [27]. Figure 4 depicts the characteristics of a semi-active damper.

EH dampers represent a modern suspension system that presents several advantages compared to their traditional counterparts. These benefits encompass heightened safety, comfort, and handling through refined wheel damping, minimized roll, pitch, and vertical movement, as well as precise maneuvering during acceleration and improved stability while cornering. EH dampers contribute to shorter braking distances by ensuring optimal road contact, continually adjusting in real-time for peak performance, and safeguarding cargo, packaging, and vehicle integrity against excessive vibration. Moreover, EH dampers can aid in diminishing road wear and tear while enhancing long-term cost efficiency. Overall, EH dampers stand as a highly efficient solution for elevating vehicle performance, comfort, and safety.

Roads can be likened to an infinite cam, characterized by a profile comprising various harmonic sine waves. This conceptualization views a vehicle's wheel as a follower, possessing vertical freedom of movement. This study employed pseudo-random excitations generated from a standard open normal distribution of intervals to replicate road profiles. Specifically, the simulation parameters included the traversal of speed bumps at a velocity of 2.57 km/h, with each bump measuring 30 mm in height. To create the road profile, a device called a signal generator produces a sine wave. The equation that defines the shape of the bumpy road is as follows:

$$Z_\circ = b - b \times (t \times t - 3)^2 \tag{21}$$

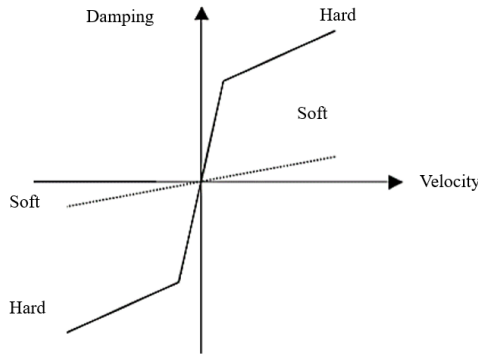where, b is the maximum amplitude of the bump, and t is the time.

Figure 4. Characteristics of a semi-active damper
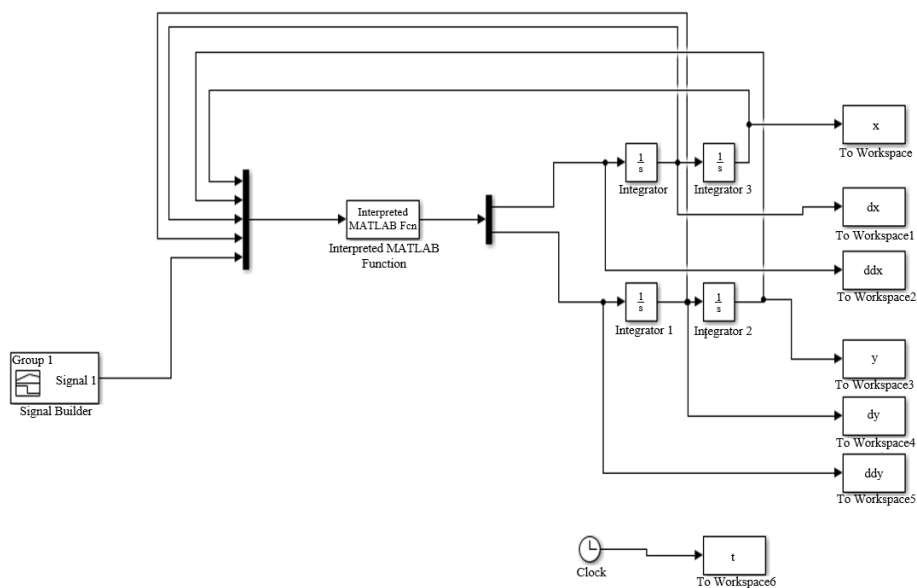

Figure 5. A diagram illustrating the simulation setup for the SASS employed

2.5 Numerical Simulation

This study focuses on evaluating passenger ride comfort as a key performance metric for vehicles traveling on bumpy roads. To achieve this, simulations were conducted using MATLAB to model passive and semi-active (using skyhook On/Off controllers) quarter-car suspension systems, as shown in Figure 5. The simulations were performed in the time domain, with a 16-second run time and a vehicle speed of 2.57 km/h. For the purpose of the simulations, specific parameters and values were selected for the quarter-car system, namely, m_s = 250 kg, m_{us} = 41 kg, k_t = 190000 N/m, k_s = 37745.6 N/m, c_1 = 2000 N.s/m, and c_1 = 1100 N.s/m [28].

3 Experiments

To assess the effectiveness of a SASS in various load conditions for a quarter-car, a quarter-car testing setup was designed and built, as shown in Figure 6. The testing apparatus comprises essential elements such as a pneumatic cylinder, solenoid valve, quick exhaust (QE) valve, Arduino Uno R3 microcontroller, load cell, data acquisition (DAQ) system, accelerometers, a photoelectric sensor, and a knock sensor.
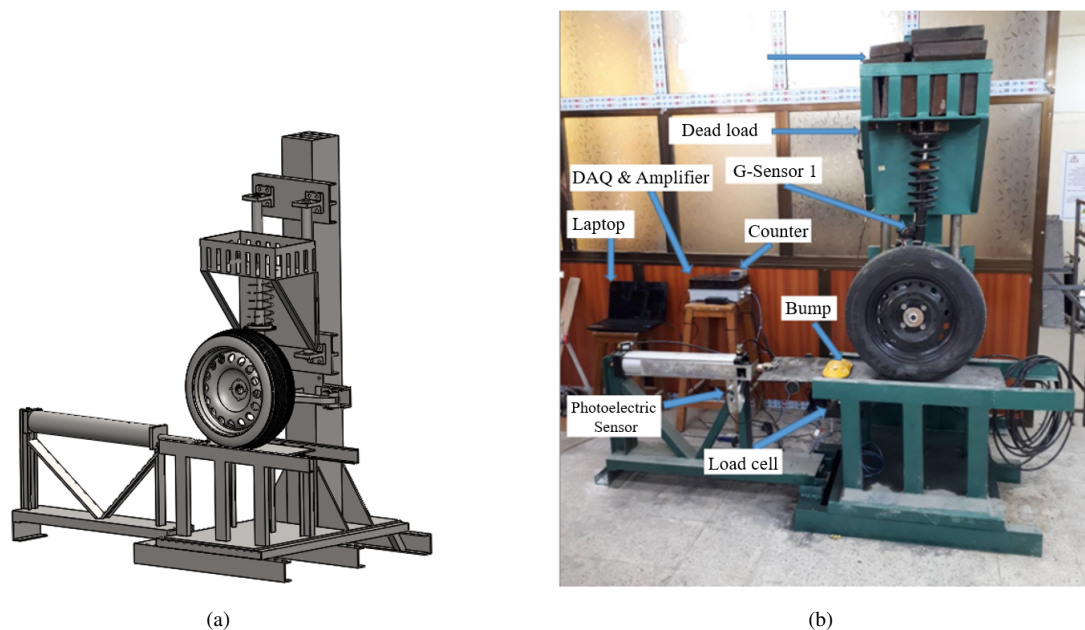

(a)   (b)

Figure 6. Experimental and SolidWorks drawings of the designed and fabricated quarter-car test rig

Pneumatic cylinder: Pneumatic actuators use compressed air to move loads along a linear path. They're preferred over hydraulic actuators because they don't leak or contaminate surrounding areas. The most popular type has a piston and rod inside a closed cylinder and can be single- or double-acting. Single-acting cylinders use one airport and an internal spring to return to their home position. Double-acting cylinders have an airport at each end, and they move the piston forward and back by alternating the high-pressure airport.

Solenoid valve: A solenoid valve is an electrically controlled valve with a movable ferromagnetic plunger at its center. When the valve is at rest, the plunger closes a small opening. When an electric current is applied to the coil, it creates a magnetic field that pulls the plunger towards the center, opening the orifice. This is the basic principle behind solenoid valve operation. The solenoid valve used is the AIRTAC model 4V410-15, with a pressure of 0.18-0.8 MPa.

QE valve: A QE valve is a device that speeds up the release of exhaust air from a pneumatic cylinder. It achieves this by diverting the exhaust air directly out of the cylinder port rather than sending it back through the control valve. To accelerate the movement of the cylinder rod in both directions, a QE valve is installed on each port of the cylinder. The OLK model QE-03 was used in this study, which operates at a pressure range of 0.05-1.0 MPa. This setup allows the cylinder to complete cycles rapidly and efficiently, resulting in enhanced performance and productivity.

Arduino Uno R3: The Arduino Uno R3 is a single-board microcontroller platform created by Arduino, a well-known open-source hardware and software company with a vast community of users. This board is utilized for constructing digital devices and interactive projects that can interact with both the physical and digital environments. Equipped with a variety of microprocessors and controllers, the board provides multiple digital and analog input/output (I/O) pins, allowing straightforward connection to a variety of expansion boards (shields) and other circuits. Some models also feature Universal Serial Bus (USB) interfaces that can be used to load programs from

personal computers (PCs). To program the microcontrollers, the Arduino project provides an integrated development environment (IDE) based on the processing language project. This IDE, which supports a dialect of features from the programming languages C and C++, is easy to use, even for beginners. With traditional compiler toolchains and the Arduino IDE, digital devices and interactive objects can be built quickly.

Load cell: For this study, a specific type of load cell known as the SS300-2ton was used. This load cell is a force-measuring transducer that detects changes in the load cell's structure using strain gauges. Strain gauges can be made from either metal foil or semiconductor materials and are highly sensitive to even small changes in the load cell's structure. As force is applied to the load cell, the strain gauges experience a proportional strain which causes an electrical resistance change. Measuring the change in resistance directly to determine strain can be a difficult task. To overcome this challenge, strain gauges are often configured in a Wheatstone bridge circuit. This circuit allows the conversion of the resistance change into a voltage change, which is a more convenient and accurate measurement.

DAQ: The USB-4431 was used as the DAQ system in this study. DAQ entails the measurement of various physical phenomena such as temperature, pressure, or sound. PC-based DAQ systems utilize both hardware and software to transform a computer into a customizable measurement or control platform. Fundamentally, all DAQ systems consist of signals, sensors, signal conditioning, DAQ hardware, and computer software. These systems facilitate the conversion of analog waveforms into digital values through the utilization of sensors, signal conditioning circuitry, and analog-to-digital converters. Furthermore, DAQ applications are managed by software programs scripted in different programming languages, with LabVIEW® being a prominent example. A DAQ system must first transform a physical property into a standardized format for accurate capture. This transformation is typically achieved using sensors, which convert physical properties into corresponding electrical signals or characteristics.

Accelerometers: The type of accelerometer employed in this context is the G-sensor. Accelerometers are utilized for two primary reasons. First, the acceleration signal is used to assess ride comfort. Second, the velocity of the car body and wheel assembly is measured and incorporated into the feedback control system. Although theoretically, an analogue or digital integrator could provide a velocity signal from an acceleration signal, numerous publications have indicated that the most convenient means of hardware realization of velocity measurement is through the use of an accelerometer.

Photoelectric sensor: To determine the piston speed, a PES-D18NOC50D photoelectric sensor was employed. This sensor functions by emitting a light beam, typically visible or infrared, from its light-emitting component. Utilizing a reflective-type photoelectric sensor, the light beam was detected upon reflection from the target. Alternatively, a thru-beam type sensor could also be employed to gauge the alteration in light intensity resulting from the target intersecting the optical axis.

Knock sensor: A knock sensor is a device that identifies engine knock or detonation by converting vibrations into an electric charge using a crystal element. When the crystal vibrates, it produces a small voltage. The knock sensor utilizes this ability to monitor engine vibrations and is often placed on the engine block, cylinder head, or intake manifold. By sensing vibrations, it transmits signals to the engine control module (ECM), which can then adjust the engine's timing to avoid potential damage.

4 Results and Discussion

4.1 Semi-Active Control Results

This section discusses the simulation results for bump and step disturbances, with the vehicle moving at 20 km/h across uneven terrain. The assessment of the SASS focuses on two key aspects: passenger comfort and system response time. Comfort is primarily evaluated through measurements of body-pitch acceleration, while stability is gauged by wheel bounce behavior. The aim is to enhance both performance measures by minimizing body and wheel bounce and associated accelerations. The suspension performance is analyzed for two distinct vibration control cases:

(i) Passive EH damper, i.e., the damper is not powered by any current or voltage at the moment.

(ii) Semi-active control with skyhook control.

The performance criteria mentioned earlier are used to quantify the relative performances of the control methods. These criteria are also used to compare the control methods with the baseline simulations conducted using MATLAB software.

This research investigates the performance of a quarter-car suspension system employing a 2-degree-of-freedom (DOF) model. The primary objective was to assess the dynamic behavior and vibration attributes of a SASS in an automotive context. Through simulation experiments conducted across different time domains, the performance of the semi-active suspension was evaluated and compared with that of both passive and skyhook semi-active suspension configurations.

A simulation was conducted in the Matlab environment to analyze the response of the SASS when it encountered a bump on the road. The obtained results are presented in Figure 7, which displays the sprung mass displacement (the subgraph (a) of Figure 7), velocity (the subgraph (b) of Figure 7), and acceleration (the subgraph (c) of Figure 7).

The tire encountered a bump at the 4.5-second mark, causing it to exceed the target by 0.026/m at 4.8 seconds and fall below the target by -0.01/m at 5.6 seconds. The system stabilized at 7.5 seconds. Similarly, the maximum overshoot and undershoot for the sprung mass velocity were 0.2 m/s and -0.23 m/s, respectively, observed at 4.6 seconds and 5.5 seconds. The system attained stability at 7.5 seconds. Additionally, the sprung mass acceleration exhibited a maximum overshoot and undershoot of 6.1 m/s^2 at 4.5 seconds and 5.4 seconds, respectively. The subgraph (c) of Figure 7 illustrates the inertia force in the system.
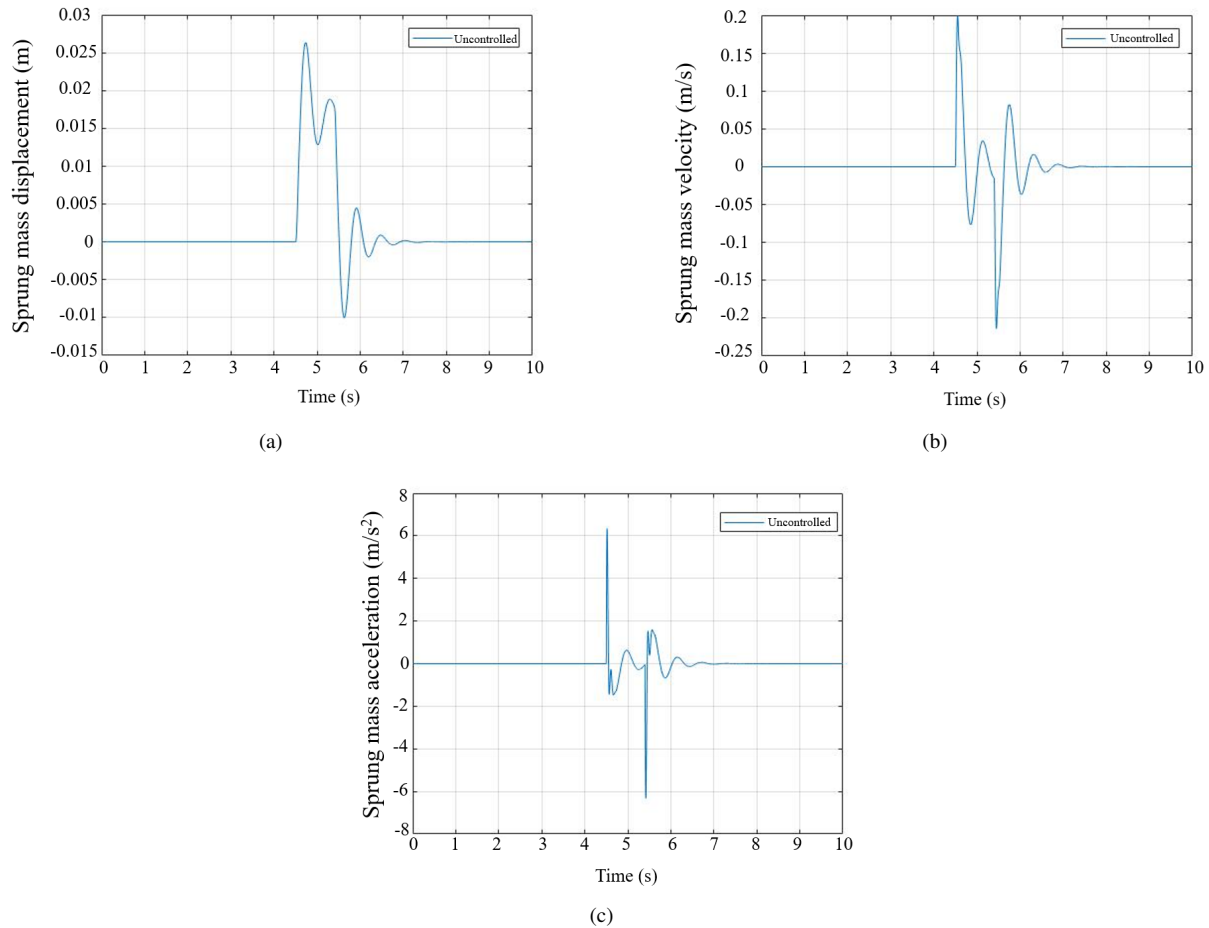

(a)

(b)

(c)

Figure 7. Displacement (a); velocity (b); acceleration (c) for sprung mass

4.2 Control Strategy Using Skyhook ON/OFF

A semi-active control strategy was suggested, which builds upon the skyhook control approach. Numerical simulation demonstrated the effectiveness of this method in regulating suspension movement during driving on uneven terrain.

The results presented in Figure 8 illustrate the behavior of the sprung mass displacement, velocity, and acceleration. The subgraph (a) of Figure 8 illustrates that the tire hits a bump at 4.5 seconds, resulting in a peak overshoot of 0.024 m at 4.8 seconds and a low point of -0.006 m at 5.3 seconds. The system regains stability at 7 seconds. In the subgraph (b) of Figure 8, the velocity of the sprung mass reaches a peak of 0.18 m/s at 4.5 seconds and a minimum of -0.149 m/s at 5.1 seconds. The subgraph (c) of Figure 8 showcases the sprung mass acceleration, with a maximum overshoot of 5.85 m/s^2 at 4.5 seconds and a minimum of -5.85 m/s^2 at 5.1 seconds.

Figure 9 shows a comparison of a SASS with and without skyhook control. The theoretical analysis reveals notable variations in displacement values when skyhook control is applied. Specifically, with skyhook control, the system demonstrates a maximum overshoot of 0.023 meters at 4.8 seconds and a maximum undershoot of -0.006 meters at 5.3 seconds. The system achieves stability within 6.6 seconds. On the other hand, the uncontrolled semi-active system shows a maximum overshoot of 0.026 m at 4.7 seconds and a maximum undershoot of -0.008m at 5.8 seconds, with a stability time of 7 seconds. The results show that the skyhook control method works better than the uncontrolled semi-active system for short-term stability and maximum overshoot displacement, which makes passengers more comfortable.
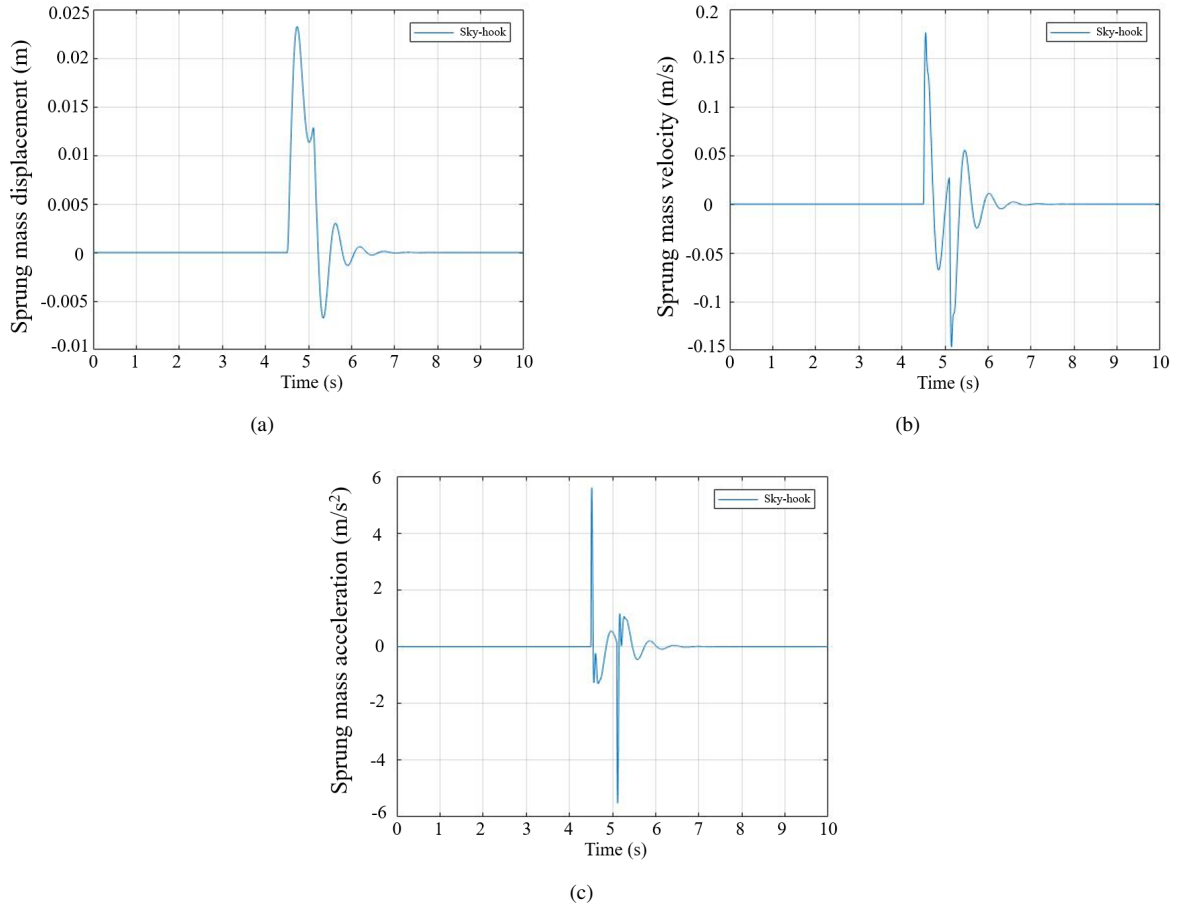
Figure 8. Displacement (a); velocity (b); acceleration (c) for sprung mass under control action
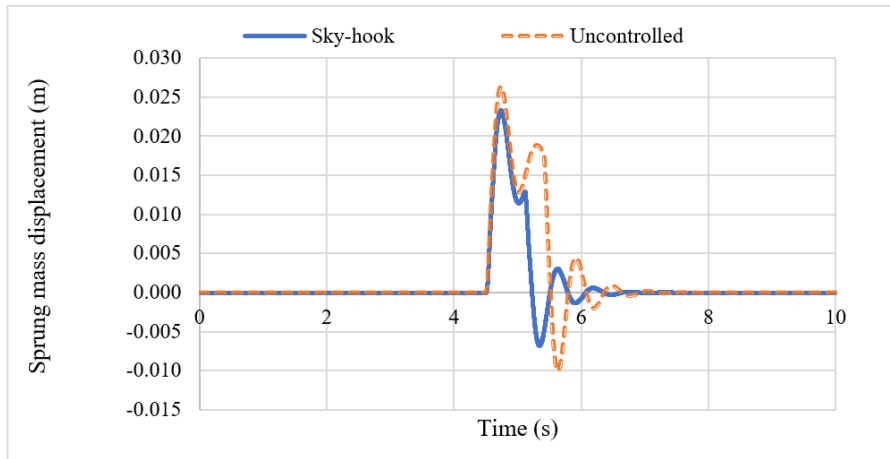

Figure 9. Theoretical result comparison between the sprung mass with and without skyhook control

The data presented in Figure 10 indicates the performance of the system with regards to unsprung mass displacement using the current control strategy. Based on the graph provided, it appears that the unsprung mass encounters a peak overshoot of 0.017m at 4.51 seconds, followed by a peak undershoot of -0.0038m at 5.1 seconds. Additionally, the stability of the unsprung mass is found to be the same as that of the sprung mass displacement, both lasting for 6.6 seconds.

Figure 11 presents the experimental comparison between a controlled and an uncontrolled SASS. The controlled system's performance is notably enhanced, showing a 20% reduction in maximum overshoot and a 27% increase in stability.
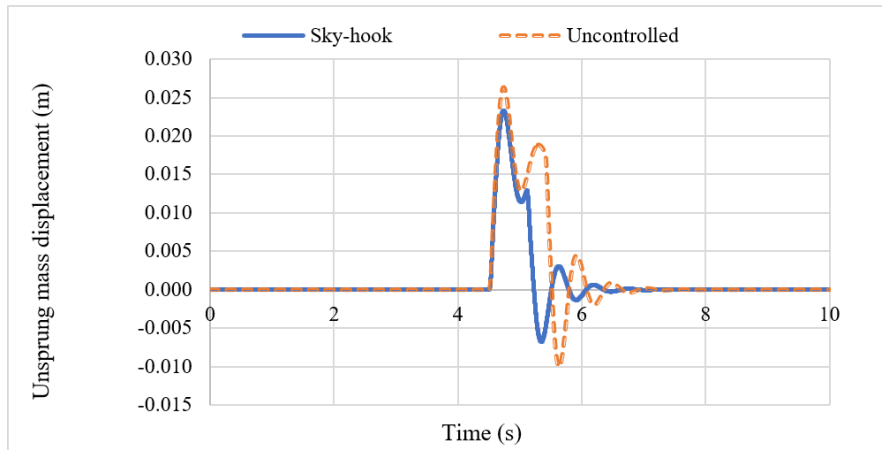
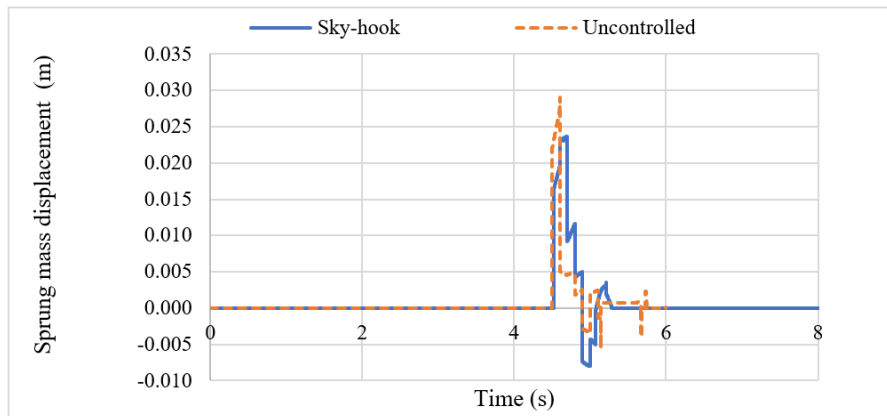**Figure 10.** Theoretical result comparison between the unsprung mass with and without skyhook control

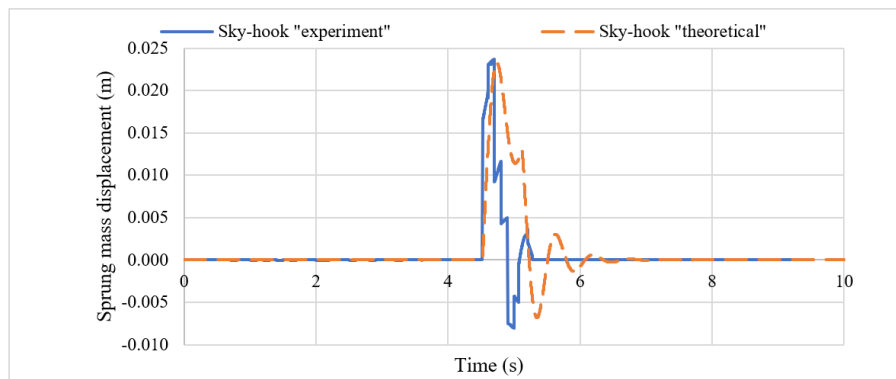**Figure 11.** Experimental comparison between the controlled and uncontrolled SASS

Figure 12. Comparison between experimental and theoretical results of the skyhook

The comparison between the experimental and theoretical results is shown in Figure 12. The displacement responses are damped to nearly time in 0.8 seconds, and the maximum overshoot is 0.0235 m in the skyhook control for the SASS model. However, the time recorded is higher (close to 4.5 seconds) for the passive suspension model. The performance of the new technique for car suspension was evaluated by comparing the values of displacement and acceleration transmissibility with those of a passive suspension. The test results showed that the developed semi-active control strategy was effective. In addition, in both experimental data and numerical simulations, the semi-active control unit achieved better performance in providing improved comfort for cars. These analyses assumed a step input for road-induced vibrations, and the percentage of error in the results was lower at high frequencies and higher at low frequencies due to noise.

To evaluate the effectiveness and performance of the controller, the proposed system was modeled in the MATLAB/Simulink environment and compared to the passive system. By utilizing continuous skyhook On/Off, the maximum overshoot of displacement decreased by 53%. The car's suspension system experienced a significant amount of deflection when it hit a speed bump. The subgraph (a) of Figure 13 shows the displacement of the car's mass over time while driving at a speed of 20 km/h. The skyhook algorithmic observer accurately estimated the suspension system's behavior as the car crossed the speed bump. The subgraph (b) of Figure 13 compares the simulation between semi-active control and passive suspension of the unsprung mass. Although the controllable suspension response and the passive one are generally similar, the former can attenuate the resonant faster than the latter. The controllable suspension is often adjusted to soft mode to constrain the excitation transmission, improving automotive comfort and stability.
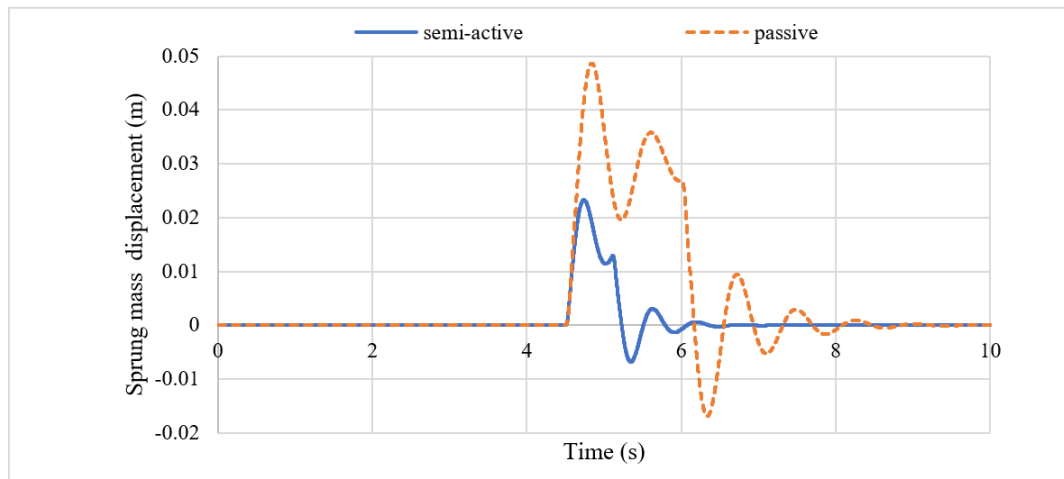
(a)
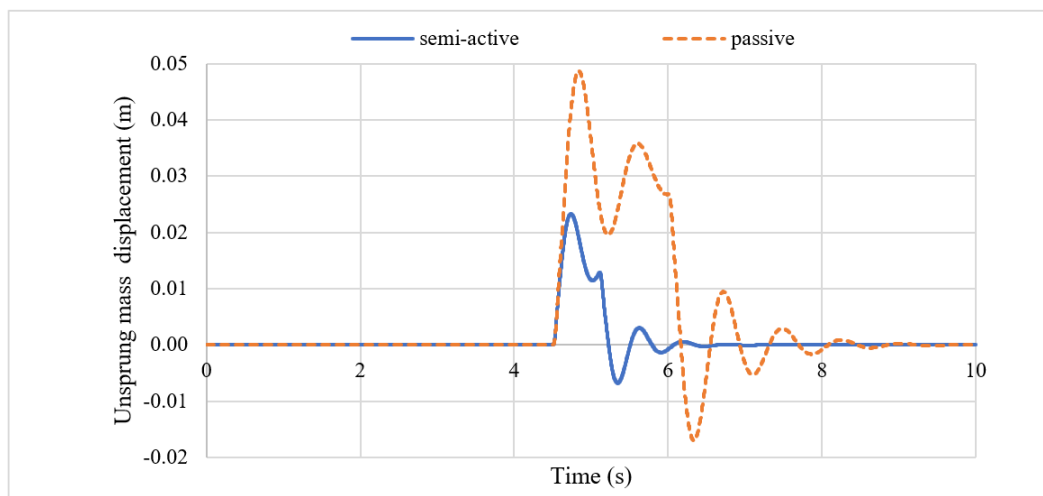
(b)

Figure 13. Comparison between the theoretical results of the semi-active suspension and the simulation of the passive suspension system for the sprung mass (a) and unsprung mass (b)

5 Conclusions

The presented research on SASSs provides important insights into both theoretical and experimental aspects of these systems. Through a full-scale test rig, the performance of a SASS was assessed in comparison to that of a passive suspension system. The results indicate that the semi-active system, utilizing EH damping and the skyhook control method, successfully reduces peak amplitude and settling time, outperforming the uncontrolled system.

The consistency between simulation and experimental data reinforces the effectiveness of the SASS. The investigation into the skyhook on/off controller revealed significant reductions in vibration and improvements in stability time. Additionally, the control strategy based on displacement performed better than the semi-active damper and

even outperformed an MR damper at higher frequencies. This research offers valuable guidance for designing and optimizing SASSs. The adaptable test rig designed for this study facilitates the evaluation of a wide range of suspension systems, both semi-active and passive, contributing to further progress in the field.

Data Availability

Not applicable.

Conflicts of Interest

The authors declare no conflict of interest.

References

[1] Y. K. Abbas, M. N. Hamzah, and S. A. Al-Samarraie, "Design of a nonlinear robust controller for vibration control of a vehicle suspension system," *Eng. Tech. J.*, vol. 29, no. 11, pp. 2259–2273, 2011. https://doi.org/10.30684/etj.29.11.14

[2] M. A. Flayyih, M. N. Hamzah, and J. M. Hassan, "Nonstandard backstepping based integral sliding mode control of hydraulically actuated active suspension system," *Int. J. Automot. Technol.*, vol. 24, pp. 1665–1673, 2023. https://doi.org/10.1007/s12239-023-0134-2

[3] D. S. Huang, J. Q. Zhang, and Y. L. Liu, "The PID semi-active vibration control on nonlinear suspension system with time delay," *Int. J. ITS Res.*, vol. 16, pp. 125–137, 2018. https://doi.org/10.1007/s13177-017-0143-5

[4] M. Z. Q. Chen, Y. L. Hu, C. Y. Li, and G. R. Chen, "Application of semi-active inerter in semi-active suspensions via force tracking," *J. Vib. Acoust.*, vol. 138, no. 4, 2016. https://doi.org/10.1115/1.4033357

[5] H. B. Ren, S. Z. Chen, Y. Z. Zhao, G. Liu, and L. Yang, "State observer-based sliding mode control for semi-active hydro-pneumatic suspension," *Veh. Syst. Dyn.*, vol. 54, no. 2, pp. 168–190, 2016. https://doi.org/10.1080/00423114.2015.1122818

[6] X. Tang, H. P. Du, S. S. Sun, D. H. Ning, Z. W. Xing, and W. H. Li, "Takagi-sugeno fuzzy control for semi-active vehicle suspension with an magneto-rheological damper and experimental validation," *IEEE/ASME Trans. Mech.*, vol. 22, no. 1, pp. 291–300, 2017. https://doi.org/10.1109/TMECH.2016.2619361

[7] K. D. Rao and S. Kumar, "Modeling and simulation of quarter-car semi active suspension system using LQR controller," in *Proceedings of the 3rd International Conference on Frontiers of Intelligent Computing: Theory and Applications (FICTA)*, 2014, pp. 441–448. https://doi.org/10.1007/978-3-319-11933-5_48

[8] M. H. Ab Talib and I. Z. Mat Darus, "Intelligent fuzzy logic with firefly algorithm and particle swarm optimization for semi-active suspension system using magneto-rheological damper," *J. Vib. Control*, vol. 23, no. 3, pp. 501–514, 2017. https://doi.org/10.1177/1077546315580693

[9] S. Gad, H. Metered, A. Bassuiny, and A. M. Abdel Ghany, "Multi-objective genetic algorithm fractional-order PID controller for semi-active magnetorheologically damped seat suspension," *J. Vib. Control*, vol. 23, no. 8, pp. 1248–1266, 2017. https://doi.org/10.1177/1077546315591620

[10] Devdutt and D. M. L. Aggarwal, "Fuzzy control of passenger ride performance using MR shock absorber suspension in quarter-car model," *Int. J. Dyn. Control*, vol. 3, pp. 463–469, 2015. https://doi.org/10.1007/s40435-014-0128-z

[11] A. Turnip and K. S. Hong, "Road-frequency based optimisation of damping coefficients for semi-active suspension systems," *Int. J. Veh. Des.*, vol. 63, no. 1, 2013. https://doi.org/10.1504/IJVD.2013.055493

[12] C. Poussot-Vassal, C. Spelta, O. Sename, S. M. Savaresi, and L. Dugard, "Survey and performance evaluation on some automotive semi-active suspension control methods: A comparative study on a single-corner model," *Annu. Rev. Control*, vol. 36, no. 1, pp. 148–160, 2012. https://doi.org/10.1016/j.arcontrol.2012.03.011

[13] J. H. Crews, M. G. Mattson, and G. D. Buckner, "Multi-objective control optimization for semi-active vehicle suspensions," *J. Sound Vib.*, vol. 330, no. 23, pp. 5502–5516, 2011. https://doi.org/10.1016/j.jsv.2011.05.036

[14] J. P. Feng, S. Y. Bei, C. Y. Yuan, and L. C. Zhang, "Research on wheelbase preview control for vehicle semi-active suspension based on neural networks," in *2009 Third International Symposium on Intelligent Information Technology Application*, Nanchang, China, 2009, pp. 290–293. https://doi.org/10.1109/IITA.2009.351

[15] X. M. Dong, M. Yu, C. R. Liao, and W. M. Chen, "Comparative research on semi-active control strategies for magneto-rheological suspension," *Nonlinear Dyn.*, vol. 59, pp. 433–453, 2010. https://doi.org/10.1007/s11071-009-9550-8

[16] M. Biglarbegian, W. Melek, and F. Golnaraghi, "A novel neuro-fuzzy controller to enhance the performance of vehicle semi-active suspension systems," *Veh. Syst. Dyn.*, vol. 46, no. 8, pp. 691–711, 2008. https://doi.org/10.1080/00423110701585420

[17] J. L. Yao and J. Q. Zheng, "Semi-active suspension system design for quarter-car model using model reference sliding mode control," in *2006 IEEE International Conference on Vehicular Electronics and Safety*, Shanghai, China, 2006, pp. 398–402. https://doi.org/10.1109/ICVES.2006.371623

[18] A. L. Do, C. Spelta, S. Savaresi, O. Sename, L. Dugard, and D. Delvecchio, "An LPV control approach for comfort and suspension travel improvements of semi-active suspension systems," in *49th IEEE Conference on Decision and Control (CDC)*, Atlanta, GA, USA, 2010, pp. 5560–5565. https://doi.org/10.1109/CDC.2010.5717271

[19] F. Yakub, P. Muhammad, Z. H. C. Daud, A. Y. A. Fatah, and Y. Mori, "Ride comfort quality improvement for a quarter-car semi-active suspension system via state-feedback controller," in *2017 11th Asian Control Conference (ASCC)*, Gold Coast, QLD, Australia, 2017, pp. 406–411. https://doi.org/10.1109/ASCC.2017.8287204

[20] R. Jayachandran and S. Krishnapillai, "Modeling and optimization of passive and semi-active suspension systems for passenger cars to improve ride comfort and isolate engine vibration," *J. Vib. Control*, vol. 19, no. 10, pp. 1471–1479, 2013. https://doi.org/10.1177/1077546312445199

[21] A. Mulla, S. Jalwadi, and D. Unaune, "Performance analysis of skyhook, groundhook and hybrid control strategies on semiactive suspension system," *Int. J. Curr. Eng. Technol.*, vol. 3.

[22] D. Karnopp, M. J. Crosby, and R. A. Harwood, "Vibration control using semi-active force generators," *J. Eng. Ind.*, vol. 96, no. 2, pp. 619–626, 1974. https://doi.org/10.1115/1.3438373

[23] Y. Chen, Z. L. Wang, J. Qiu, and H. Z. Huang, "Hybrid fuzzy skyhook surface control using multi-objective microgenetic algorithm for semi-active vehicle suspension system ride comfort stability analysis," *J. Dyn. Sys., Meas., Control.*, vol. 134, no. 4, p. 041003, 2012. https://doi.org/10.1115/1.4006220

[24] X. B. Song, "Cost-effective skyhook control for semiactive vehicle suspension applications," *Open Mech. Eng. J.*, vol. 3, pp. 17–25, 2009. https://doi.org/10.2174/1874155X00903010017

[25] B. A. R. Abdullah, M. N. Hamzah, and A. S. Merza, "Design and control of a full-scale quarter-car test rig for semi-active suspension system," *Eng. Technol. J.*, vol. 37, no. 10A, pp. 416–421, 2019. https://doi.org/10.30684/etj.37.10A.6

[26] E. Guglielmino, T. Sireteanu, C. W. Stammers, G. Ghita, and M. Giuclea, *Semi-active Suspension Control: Improved Vehicle Ride and Road Friendliness*. Springer Science and Business Media, 2008.

[27] G. Z. Yao, F. F. Yap, G. Chen, W. H. Li, and S. H. Yeo, "MR damper and its application for semi-active control of vehicle suspension system," *Mechatronics*, vol. 12, no. 7, pp. 963–973, 2002. https://doi.org/10.1016/S0957-4158(01)00032-0

[28] N. Gupta, "Development of semi-active control system for hydraulic dampers," mastersthesis, 2015.

Nomenclature

A	The state matrix
B	The input matrix
c	Damping coefficient (N.s/m)
$C_{\max}$	The damper maximum damping coefficients
$C_{\min}$	The damper minimum damping coefficients
C	The output matrix
D	The direct transmission matrix
F_{sky}	Skyhook force (N)
k_s	Stiffness of car body spring (N/m)
k_t	Stiffness of tire (N/m)
m_s	Sprung mass (kg)
m_{us}	Unsprung mass (kg)

Greek symbols

α	thermal diffusivity, $m^2{\cdot}s^{-1}$
β	thermal expansion coefficient, K^{-1}
ϕ	solid volume fraction
σ	dimensionless temperature
μ	dynamic viscosity, $kg{\cdot}m^{-1}{\cdot}s^{-1}$

Subscripts

ξ	The shape and size of the tube that connects the valves with the compression or rebound chamber